Featured in Physics

Curvature as a Guiding Field for Patterns in Thin Block Copolymer Films

Giang Thi Vu,[1,*] Anabella A. Abate,[2] Leopoldo R. Gómez,[2] Aldo D. Pezzutti,[2]
Richard A. Register,[3] Daniel A. Vega,[2,†] and Friederike Schmid[1,‡]
[1]*Institut für Physik, Johannes Gutenberg Universität Mainz Staudinger Weg 7, D-55099 Mainz, Germany*
[2]*Department of Physics, Universidad Nacional del Sur—IFISUR CONICET, 800, Bahia Blanca, Argentina*
[3]*Department of Chemical and Biological Engineering, Princeton University, Princeton, New Jersey 08544, USA*

(Received 14 February 2018; revised manuscript received 13 June 2018; published 21 August 2018)

Experimental data on thin films of cylinder-forming block copolymers (BC)—free-standing BC membranes as well as supported BC films—strongly suggest that the local orientation of the BC patterns is coupled to the geometry in which the patterns are embedded. We analyze this phenomenon using general symmetry considerations and numerical self-consistent field studies of curved BC films in cylindrical geometry. The stability of the films against curvature-induced dewetting is also analyzed. In good agreement with experiments, we find that the BC cylinders tend to align along the direction of curvature at high curvatures. At low curvatures, we identify a transition from perpendicular to parallel alignment in supported films, which is absent in free-standing membranes. Hence both experiments and theory show that curvature can be used to manipulate and align BC patterns.

DOI: 10.1103/PhysRevLett.121.087801

Because of their ability to self-assemble into well-defined periodic nanostructures, block copolymers (BC) are attracting great interest as potential template materials for cost-effective nanofabrication techniques [1–9]. With BC systems, one can produce high-resolution patterns with tunable wavelength using traditional processing techniques. This offers promising perspectives for applications in scalable nanoscale devices. However, one frequent problem with the self-assembly approach is lack of long-range order due to pattern undulations and defects, e.g., dislocations, disclinations, or grain boundaries [1,10–13]. Numerous methods to produce patterns with well-defined orientational and positional order have been proposed, such as shear alignment [14–16], alignment in electric fields [17–19], zone annealing [20,21], or grapho- and chemoepitaxy, where surface interactions and confinement effects are exploited to order patterns [6–8,14,21–27] or to control defect positions [28].

Here, we analyze another possible source of alignment, the *geometry* in which the system is embedded. Experiments and simulations on curved systems have indicated that the pattern configurations are affected by both intrinsic and extrinsic geometry. Even in Euclidean systems, a strong coupling between patterns and curvature seems to drive the equilibrium configurations and the coarsening process [7,23,29,30].

As a first step towards a more quantitative understanding of the nature of the coupling between BC thin films or membranes and curvature, in the present Letter, we study curved monolayers of cylinder-forming BC systems by complementary experiments, symmetry considerations, and self-consistent field theory (SCFT) calculations [9,31]. We consider two types of model systems: (a) free-standing BC membranes and (b) BC thin films deposited onto a curved substrate.

The geometric features of a 2D curved surface can be characterized in terms of a shape operator $\mathbf{S}$, which has two Eigenvalues $k_{1,2} = 1/R_{1,2}$ corresponding to the inverse maximal and minimal radii of curvature R_i (see Supplemental Material [32] for more details). The determinant and the trace of $\mathbf{S}$ define the Gaussian curvature $K = k_1 k_2$ and twice the mean curvature $2H = k_1 + k_2$, respectively [33]. The experimental systems studied here have a non-Euclidean metric ($K \neq 0$, free-standing membrane) or a Euclidean metric with zero Gaussian curvature ($K = 0$, curved substrate).

In both systems we employ the same BC system, a cylinder-forming polystyrene-block-poly(ethylene-alt-propylene) diblock (PS-PEP 4/13) [34]. The number-average block molecular weights for the BC are 4.3 kg/mol for PS and 13.2 kg/mol for PEP. In bulk, the PS blocks arrange in hexagonally packed cylinders embedded in the PEP matrix. In thin films the PS cylinders adopt a configuration parallel to the film surface. The center-to-center spacing of the cylinders is $d_{\mathrm{sm}} = 21$ nm. Thin films of thickness ~30 nm are prepared by spin coating from a 1 wt. % solution in toluene, a good solvent for both blocks. Order is induced by annealing at a temperature T, above the glass transition of the PS block ($T_g \sim 330$ K) and below the order-disorder transition temperature $T_{\mathrm{ODT}} = 417$ K of the BC. Details of the preparation of the experimental systems are given in the Supplemental Material [32]. To obtain free-standing membranes, the films are first annealed on a flat substrate, then further cooled down below the T_g of the PS block and finally lifted off and redeposited on a transmission electron

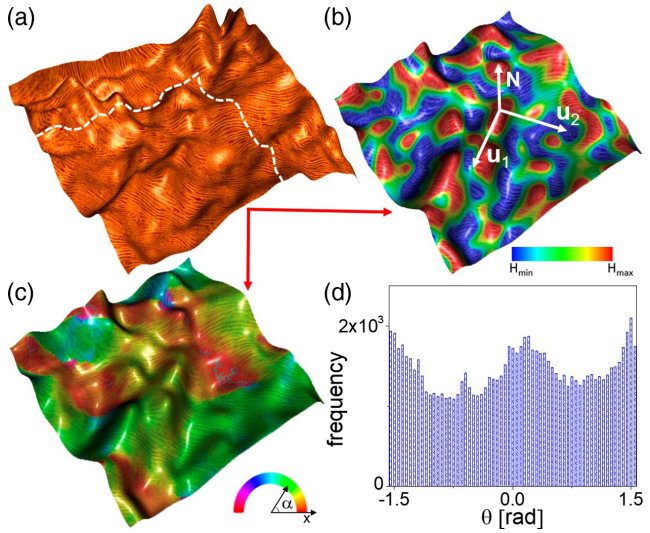

FIG. 1. (a) Phase-height AFM image of a free-standing thin film (image size: 2.6 μm $\times$ 2.6 μm). (b) Local mean curvature for the membrane shape. Here the vectors $u_{1,2}$ indicate the directions of the principal curvatures and $\mathbf{N}$ is the normal vector to the membrane surface (image size: 1.8 μm $\times$ 1.8 μm, region indicated by dashed lines in panel a; $H_{\max} = -H_{\min} = 3.84 \times 10^{-3}$ nm^{-1}). (c) Local orientation of the director field α of the pattern with regard to the x axis. (d) Histogram showing the local distribution of angles $\theta = \alpha - \beta$ between α and the local orientation of the membrane wrinkles β (see also Fig. S2 in the Supplemental Material [32]).

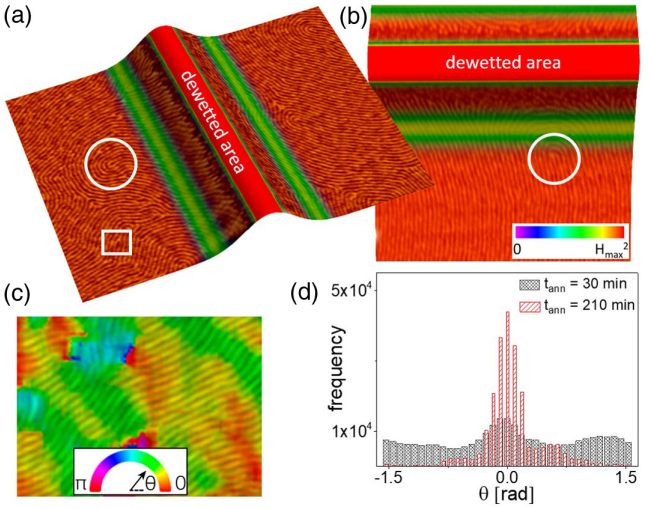

FIG. 2. Top panels: 3D AFM phase-height images of the BC thin film on a curved substrate after annealing at $T = 373$ K. Panels (a) and (b) show the pattern configuration after 90 min (image size: 2.0 μm $\times$ 1.5 μm) and 3.5 h of thermal annealing (image size: 1.0 μm $\times$ 1.25 μm), respectively. Height scale: 80 nm from crest to valley, $H^2_{\max} = 6.25$ μm^{-2}. The presence of a dislocation and $+1/2$ disclinations has been emphasized with a rectangle and circles, respectively. Bottom panels: (c) Local orientation of the smectic pattern (color map indicated at the bottom). (d) Histograms showing the distribution of angles θ between the local cylinder orientation and the direction of curvature at two different annealing times.

microscopy (TEM) grid. During this process, the system retains the symmetry, average intercylinder distance, and structure of defects established during annealing. To obtain supported films, the BCs are directly spin coated onto curved substrates and the thermal annealing process is monitored by atomic force microscopy (AFM) at selected time points.

Figure 1 shows an AFM image of a free-standing film where height and cylinder locations are measured simultaneously. The light and dark regions correspond to PS-rich and PEP-rich regions, respectively. After releasing the membrane from the confining substrate, it develops a non-Euclidean shape to relieve the elastic energy of topological defects that have survived the thermal annealing. The shape results from a competition between the strain field of the defects, the bending energy associated with the curvature of the membrane, and the membrane tension [29]. Figure 1(d) shows the correlation between the orientation of the underlying pattern and the local orientation of membrane wrinkles. Although the different defects impose competing out-of-plane deformations, one clearly notices that wrinkles have a tendency to be oriented either perpendicular ($\theta = 0$) or parallel ($\theta = \pm\pi/2$) to the underlying cylinders, suggesting that the bending energy is anisotropic and coupled to the liquid crystalline order of the BC (see also Figs. S3, S4 in the Supplemental Material [32]).

A similar observation is made for the thin films on curved substrates. Figure 2 shows AFM phase and height-phase images of the BC thin film deposited onto a curved substrate. Right after the spin coating, the pattern is characterized by a very small orientational correlation length ($\xi_2 \sim 20$ nm) and a high density of defects. During annealing at $T = 373$ K, the system orders via annihilation of dislocations and disclinations. Already at an early stage of annealing, the thin film becomes unstable and dewets at the regions with the highest curvature (Fig. 2). Upon further annealing, the order in the system increases and the pattern develops a clear preferential orientation with regard to the substrate. Figure 2 shows that the PS cylinders tend to align perpendicular to the crest of the substrate. Thus the topography of the substrate seems to act as an external field that breaks the azimuthal symmetry (see also Fig. S5 in the Supplemental Material [32]). Note that the equilibrium configuration obtained here is opposite to that predicted in previous theories for curved columnar phases [35,36], where it was assumed that bending along the cylinder direction is energetically more costly than bending in the perpendicular direction [36].

The phenomena described above can be analyzed using general symmetry considerations. The curvature free energy per area of *isotropic* fluidlike membranes can be expanded in the invariants of the shape operator $\mathbf{S}$ as $F_{\mathrm{HC}} = (\kappa_b/2)(2H - c_0)^2 + \kappa_g K$, where κ_b and κ_g are the

bending and Gaussian rigidity, respectively, and c_0 is the spontaneous curvature [37,38]. Here we consider anisotropic *nematic* membranes with in-plane order characterized by a director $\mathbf{n}$ (the orientation of the cylinders); thus additional terms become possible. Including all terms up to second order in $\mathbf{S}$ that are compatible with the in-plane nematic symmetry, i.e., $(\mathbf{n}\cdot\mathbf{S}\cdot\mathbf{n})$, $(\mathbf{n}\cdot\mathbf{S}\cdot\mathbf{n})^2$ [39,40], and $(\mathbf{S}\cdot\mathbf{n})^2$ [41,42], we can derive the following expression for the anisotropic part of the curvature free energy per area (see the Supplemental Material [32]):

$$F_{\mathrm{ani}} = -\frac{\kappa'}{2}(k_1-k_2)(2H-c_0')\cos(2\theta) - \frac{\kappa''}{2}(H^2-K)\cos(4\theta). \quad (1)$$

Here, $\theta \in [0:\pi/2]$ denotes the angle between the director and the direction of largest curvature k_1 ($|k_1| > |k_2|$), and κ', κ'', c_0' are anisotropic elastic parameters. In symmetric membranes, c_0' vanishes ($c_0' = 0$). We emphasize that Eq. (1) gives the generic form of the free energy of curved nematic films up to second order in the curvatures, which should be generally valid regardless of molecular details. For $\kappa'' > 0$, the second term describes a quadrupolar coupling between the curvature tensor and the director that favors *two* directions of preferential alignment of the director $\mathbf{n}$ along the two principal directions of curvature. Such a competition between two stable and metastable aligned states was also predicted in other continuum models for nematic shells [43,44]. The first term selects between the two directions.

The results of the symmetry analysis are compatible with the experiments: As discussed above, in the BC membranes, wrinkles form preferentially parallel or perpendicular to the director [Fig. 1(d)]. Similarly, in the thin films, the distribution of local cylinder orientations θ is bimodal at early annealing time (30 min), with two characteristic peaks separated by $\sim\pi/2$ [Fig. 2(d)]. During the first stage of coarsening, the parallel and perpendicular configurations compete. After long annealing times, $C_\perp$ dominates, and the histogram becomes sharply peaked at the orientation $\theta = 0$, suggesting $\kappa' > 0$ in Eq. (1). We note, however, that supported films are asymmetric and hence the spontaneous curvature parameter c_0' will very likely not vanish, in which case Eq. (1) predicts that the preferred orientation switches from $\theta = 0$ to $\theta = \pi/2$ in a region of very small curvatures $k_1 \in [0:c_0']$. We will discuss this further below.

In order to obtain a more quantitative theoretical description, we use SCFT [31,45] to study the two systems considered in the experiment, the free-standing membrane and the curved supported thin film. We consider a melt of asymmetric AB diblock copolymer molecules with degree of polymerizaton N and statistical segment length b at temperature T confined to a curved film of thickness ϵ

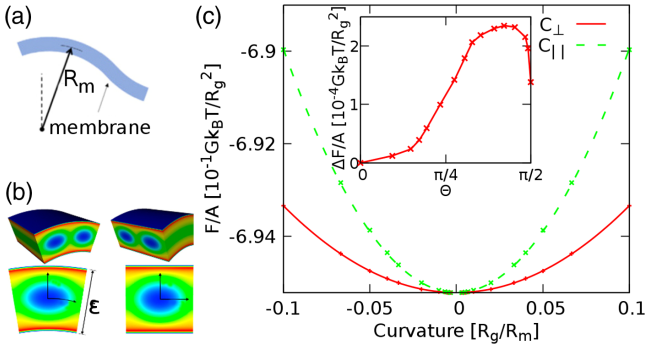

FIG. 3. (a) Schematic representation of curvature radius R_m in free-standing membranes. (b) Density profiles from SCFT for the parallel (left) and perpendicular (right) configurations $C_\parallel$ and $C_\perp$ at $R_m = 9Rg$. (c) Free energy per area as a function of inverse curvature radius R_g/R_m for the $C_\parallel$ and $C_\perp$ configurations. Inset shows the free energy shift per area as a function of angle θ between the cylinders and the direction of curvature relative to the $C_\perp$ configuration ($\theta = 0$) at $R_m = 50R_g$.

by two coaxial cylindrical surfaces [see schematics in Figs. 3(a), 4(a), and 4(b)]. Periodic or tilted periodic boundary conditions (see the Supplemental Material [32]) are applied in the two in-plane directions.

In the following, lengths and energies are given in units of $R_g^2 = \frac{1}{6}Nb^2$ and Gk_BT, respectively, where k_B is the Boltzmann constant and $G = \rho_c R_g^3$ is the rescaled dimensionless copolymer density in the bulk. The incompatibility between the blocks is specified by the product χN, where χ is the Flory-Huggins parameter. Here we use $\chi N = 20$ and $f = 0.7$ to match the experimental values (f is the volume fraction of the A block). Our calculations are done in the grand canonical ensemble with the chemical potential $\mu = (2.55 + \ln G)k_BT$ [9,46] and inverse isothermal compressibility $\kappa N = 25$ [47–49]. Monomers $\alpha = A$, B close to a surface experience a surface field, which we characterize in terms of the surface energy per area γ_α of a fluid of α monomers in contact with the same surface (see the Supplemental Material [32]), given in units $\hat{\gamma} = Gk_BT/R_g^2$. To account for the experimental fact that cylinders align parallel to the film, the interaction parameters are chosen such that majority A blocks preferentially adsorb to the surface, i.e., $\gamma_A < \gamma_B$. In planar films, the copolymers then self-assemble into aligned cylinders with a spacing $\lambda = 3.6R_g$. Matching this with the value $d_{\mathrm{sm}} = 21$ nm observed experimentally, we can identify $R_g \approx 5.8$ nm [50] and hence $G = 5.77$ for our experimental systems (assuming an average copolymer density of $0.861\,\mathrm{g/cm^3}$ at 363 K).

We first consider free-standing membranes, which we model as a symmetric film with surface interaction energies $\gamma_A N = -24\hat{\gamma}$ and $\gamma_B N = -23\hat{\gamma}$. We calculate the free energy per area as a function of the curvature radius $1/R_m$ of the mid-surface of the film [see Fig. 3(a)] for the two cases where cylinders are aligned parallel or

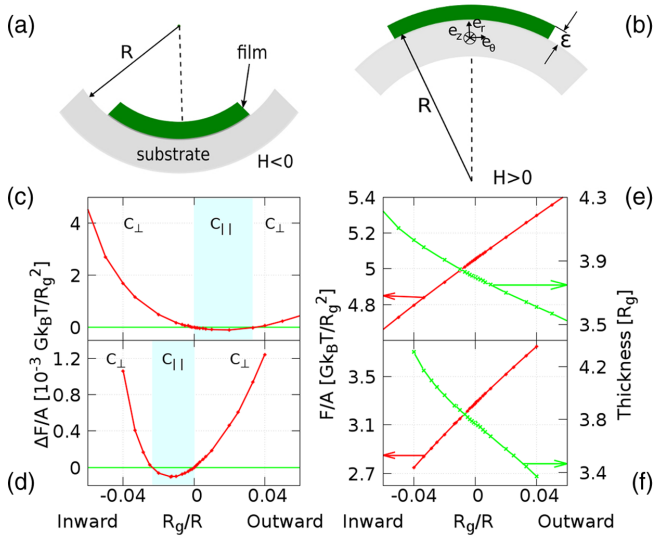

FIG. 4. (a),(b) Schematic representation of supported thin films (green) on curved substrates (gray). (c,d) Free energy difference per area $\Delta F = (F_{||} - F_{\perp})/A$ of supported thin films with parallel ($C_{||}$) vs perpendicular ($C_{\perp}$) orientation, versus curvature, for two sets of surface interaction energies I (top) and II (bottom) as described in the main text. Blue shaded regions highlight curvature regimes where the parallel orientation is more favorable ($\Delta F < 0$). (e),(f) Corresponding curves for the free energy per area (red) and thickness (green) in the perpendicular configuration $C_{\perp}$.

perpendicular to the curvature [$C_{||}$, $C_{\perp}$, see Fig. 3(b)]. In each case, the film thickness ϵ and the wavelength of the characteristic pattern are optimized to obtain the lowest free energy state. Figure 3(b) shows the resulting density profiles for the parallel and perpendicular configurations in a system with a relatively large curvature ($R_m = 9Rg$). The differences are small, indicating that curvature affects neither the position of the cylinder with regard to the plane of symmetry, nor the segregation strength. The optimum intercylinder spacing is $\lambda \sim 3.6R_g$, which is slightly smaller than the bulk value, $\lambda_{\text{bulk}} \sim 3.7R_g$. The ratio, $\lambda/\lambda_{\text{bulk}} \sim 0.97$, is in good agreement with SCFT calculations and experiments on flat substrates, where it was found that in thin films the unit cell is stretched perpendicular to the plane of the film resulting in lateral distances smaller than those in bulk [9,53]. The optimal thickness is $\epsilon \sim 3.5R_g$ for both the parallel and perpendicular configurations (see Fig. S9 in the Supplemental Material [32]). None of these features appears to be severely affected by the curvature within the range of curvatures explored here.

The behavior of the free energy per area for the two configurations is shown in Fig. 3(c). The perpendicular orientation is clearly favored. Furthermore, in agreement with Eq. (1), both $C_{\perp}$ and $C_{||}$ represent local free energy minima with respect to variations of the angle θ between cylinders and the direction of curvature (see inset of Fig. 3c). Since the free energy grows almost quadratically with the curvature, $F/A = \kappa/2R_m^2$, we can calculate bending stiffness parameters for the $C_{||}$ and $C_{\perp}$ configurations. By fitting the free energy per area up to a quadratic order of the mean curvature, we obtain $\kappa_{||} = (1.056 \pm 0.002)Gk_BT$ and $\kappa_{\perp} = (0.376 \pm 0.002)Gk_BT$ for the parallel and perpendicular configurations, respectively. Comparing this with Eq. (1) and using $k_1 = \pm 1/R_m$, $k_2 = 0$, we can deduce $\kappa' = (\kappa_{||} - \kappa_{\perp}) = 0.68Gk_BT \approx 4k_BT$, which corresponds to $\kappa' \approx 1.6 \times 10^{-13}$ erg at room temperature. In contrast, the total bending energy of the membranes has been estimated to be of order $\kappa_b \sim 10^{-9}$ erg, which is much higher due to the large contribution of the glassy PS block [29]. Hence, the influence of κ' on the membrane shapes is presumably negligible.

The situation is different when looking at copolymer ordering in supported films, where the curvatures are kept fixed and energy differences of order k_BT do significantly influence the selection of the pattern orientations.

Thin films differ from membranes in two respects. First, the reference surface which is kept fixed during the free energy minimization is the interface between the substrate and the film (not the midplane of the film as in membranes), and second, the interaction energies may be different at the substrate and air interfaces. Figures 4(c),4(d) shows results for $\gamma_B^{a,s} = -6\hat{\gamma}$ and two representative parameter sets for $\gamma_A^{a,s}$: (I) $\gamma_A^s N = -10\hat{\gamma}$, $\gamma_A^a N = -20\hat{\gamma}$, and (II) $\gamma_A^s N = -24\hat{\gamma}$, $\gamma_A^a N = -10\hat{\gamma}$, where superscripts s and a denote "substrate" and "air," respectively. In both cases, the perpendicular configuration is more favorable at large curvatures. At small curvatures, however, there exists a small regime where parallel configurations have lower free energy. This is in agreement with our symmetry considerations [see above, Eq. (1)] and also with the experimental observations. Indeed, Fig. 2(b) and Fig. S3 in the Supplemental Material [32] suggest that the locally preferred orientation switches from perpendicular to parallel in a region around the inflection point of the surface profile (green shaded areas in Fig. 2), and this induces defects in that region. Hence curvature can be used not only to orient patterns, but also to generate defects at specific regions in space.

Figure 4 also shows the behavior of the free energy and the minimum-energy thickness as a function of mean curvature for the $C_{\perp}$ configuration. For $H \geq 0$, the free energy increases as the curvature increases, indicating that the thin film is likely to become unstable and dewet from the substrate, also in good agreement with the experimental data shown in Fig. 2. Conversely, for $H < 0$ the film remains stable, since the free energy decreases as the curvature increases. In the experiments (Fig. 2), it can be observed that the thin film dewets at the region with the highest curvature, where $H_{\max}R_g \sim 0.015$. These results are in good agreement with recent experiments on curved substrates by Park and Tsarkova [54], who also found dewetting for $H > 0$ and thin film thickening for $H < 0$ in agreement with Figs. 4(e),4(f) (green curves).

In conclusion, we have shown through experiments, symmetry considerations, and SCFT calculations that curvature can be employed as a guiding field to produce well-ordered patterns. The SCFT calculations provide a rough estimate of the equilibrium configuration for curved systems and predict dewetting in regions with high local positive curvature $H > 0$. From a technological perspective, our results indicate that through appropriate control over the surface interactions, it should be possible to prevent dewetting while keeping a geometric field with sufficient strength to guide order.

We gratefully acknowledge the financial support from the Deutsche Forschungsgemeinschaft (Grants No. Schm 985/19 and No. SFB TRR 146), the National Science Foundation MRSEC Program through the Princeton Center for Complex Materials (DMR-1420541), the Universidad Nacional del Sur, and the National Research Council of Argentina (CONICET). The SCFT calculations were done on the high performance computing center MOGON in Mainz. PS-PEP 4/13 was synthesized by Dr. Douglas Adamson.

*gianthvu@uni-mainz.de
†dvega@uns.edu.ar
‡friederike.schmid@uni-mainz.de

[1] C. Harrison, D. H. Adamson, Z. D. Cheng, J. M. Sebastian, S. Sethuraman, D. A. Huse, R. A. Register, and P. M. Chaikin, Science **290**, 1558 (2000).
[2] R. A. Segalman, Mater. Sci. Eng. R **48**, 191 (2005).
[3] I. Bita, J. K. W. Yang, Y. S. Jung, C. A. Ross, E. L. Thomas, and K. K. Berggren, Science **321**, 939 (2008).
[4] R. Ruiz, H. Kang, F. A. Detcheverry, E. Dobisz, D. S. Kercher, T. R. Albrecht, J. J. de Pablo, and P. F. Nealey, Science **321**, 936 (2008).
[5] G. Singh, K. G. Yager, B. Berry, H.-C. Kim, and A. Karim, ACS Nano **6**, 10335 (2012).
[6] A. P. Marencic and R. A. Register, Annu. Rev. Chem. Biomol. Eng. **1**, 277 (2010).
[7] D. A. Vega, L. R. Gómez, A. D. Pezzutti, F. Pardo, P. M. Chaikin, and R. A. Register, Soft Matter **9**, 9385 (2013).
[8] N. A. García, A. D. Pezzutti, R. A. Register, D. A. Vega, and L. R. Gómez, Soft Matter **11**, 898 (2015).
[9] A. A. Abate, G. T. Vu, A. D. Pezzutti, N. A. García, R. L. Davis, F. Schmid, R. A. Register, and D. A. Vega, Macromolecules **49**, 7588 (2016).
[10] C. Harrison, Z. Cheng, S. Sethuraman, D. A. Huse, P. M. Chaikin, D. A. Vega, J. M. Sebastian, R. A. Register, and D. H. Adamson, Phys. Rev. E **66**, 011706 (2002).
[11] D. A. Vega, C. K. Harrison, D. E. Angelescu, M. L. Trawick, D. A. Huse, P. M. Chaikin, and R. A. Register, Phys. Rev. E **71**, 061803 (2005).
[12] U. Nagpal, M. Müller, P. F. Nealey, and J. J. de Pablo, ACS Macro Lett. **1**, 418 (2012).
[13] S.-M. Hur, V. Thapar, A. Ramírez-Hernández, G. Khaira, T. Segal-Peretz, P. A. Rincon-Delgadillo, W. Li, M. Müller, P. F. Nealey, and J. J. de Pablo, Proc. Natl. Acad. Sci. U.S.A. **112**, 14144 (2015).
[14] D. E. Angelescu, J. H. Waller, D. H. Adamson, P. Deshpande, S. Y. Chou, R. A. Register, and P. M. Chaikin, Adv. Mater. **16**, 1736 (2004).
[15] S. Y. Kim, A. Nunns, J. Gwyther, R. L. Davis, I. Manners, P. M. Chaikin, and R. A. Register, Nano Lett. **14**, 5698 (2014).
[16] R. L. Davis, B. T. Michal, P. M. Chaikin, and R. A. Register, Macromolecules **48**, 5339 (2015).
[17] K. Amundson, E. Helfand, X. Quan, and S. D. Smith, Macromolecules **26**, 2698 (1993).
[18] T. L. Morkved, M. Lu, A. M. Urbas, E. E. Ehrichs, H. M. Jaeger, P. Mansky, and T. P. Russell, Science **273**, 931 (1996).
[19] P. Mansky, J. DeRouchey, T. P. Russell, J. Mays, M. Pitsikalis, T. Morkved, and H. Jaeger, Macromolecules **31**, 4399 (1998).
[20] B. C. Berry, A. W. Bosse, J. F. Douglas, R. L. Jones, and A. Karim, Nano Lett. **7**, 2789 (2007).
[21] K. G. Yager, N. J. Fredin, X. Zhang, B. C. Berry, A. Karim, and R. L. Jones, Soft Matter **6**, 92 (2010).
[22] S. O. Kim, H. H. Solak, M. P. Stoykovich, N. J. Ferrier, J. J. de Pablo, and P. F. Nealey, Nature (London) **424**, 411 (2003).
[23] L. R. Gómez and D. A. Vega, Phys. Rev. E **79**, 031701 (2009).
[24] N. A. García, R. L. Davis, S. Y. Kim, P. M. Chaikin, R. A. Register, and D. A. Vega, RSC Adv. **4**, 38412 (2014).
[25] M. Luo, D. M. Scott, and T. H. Epps III, ACS Macro Lett. **4**, 516 (2015).
[26] D. Sundrani, S. B. Darling, and S. J. Sibener, Nano Lett. **4**, 273 (2004).
[27] I. W. Hamley, Prog. Polym. Sci. **34**, 1161 (2009).
[28] D. R. Nelson, Nano Lett. **2**, 1125 (2002).
[29] E. A. Matsumoto, D. A. Vega, A. D. Pezzutti, N. A. García, P. M. Chaikin, and R. A. Register, Proc. Natl. Acad. Sci. U.S.A. **112**, 12639 (2015).
[30] A. D. Pezzutti, L. R. Gómez, and D. A. Vega, Soft Matter **11**, 2866 (2015).
[31] M. Müller and F. Schmid, Adv. Polym. Sci. **185**, 1 (2005).
[32] See Supplemental Material at http://link.aps.org/supplemental/10.1103/PhysRevLett.121.087801 for a more detailed description of the experimental systems, additional theoretical derivations and a brief summary of the SCF equation.
[33] M. Deserno, *Handbook of Modern Biophysics: Membrane Elasticity and Mediated Interactions in Continuum Theory: A Differential Geometric Approach* (Humana Press, New York, 2009).
[34] A. P. Marencic, D. H. Adamson, P. M. Chaikin, and R. A. Register, Phys. Rev. E **81**, 011503 (2010).
[35] C. D. Santangelo, V. Vitelli, R. D. Kamien, and D. R. Nelson, Phys. Rev. Lett. **99**, 017801 (2007).
[36] R. D. Kamien, D. R. Nelson, C. D. Santangelo, and V. Vitelli, Phys. Rev. E **80**, 051703 (2009).
[37] W. Helfrich, Z. Naturforsch. C **28**, 693 (1973).
[38] P. B. Canham, J. Theor. Biol. **26**, 61 (1970).
[39] T. Powers and P. Nelson, J. Physique II **5**, 1671 (1995).
[40] P. Biscari and E. M. Terentjev, Phys. Rev. E **73**, 051706 (2006).

[41] R. Oda, I. Huc, M. Schmutz, S. J. Candau, and F. C. MacKintosh, Nature (London) **399**, 566 (1999).
[42] C.-M. Chen, Phys. Rev. E **59**, 6192 (1999).
[43] G. Napoli and L. Vergori, Phys. Rev. Lett. **108**, 207803 (2012).
[44] G. Napoli and L. Vergori, Phys. Rev. E **85**, 061701 (2012).
[45] M. W. Matsen, J. Phys. Condens. Matter **14**, R21 (2002).
[46] In Ref. [9], $\mu = (2.5 + \ln G)k_B T$ was used. Here we had to slightly increase μ, otherwise films on curved substrates with positive curvature were not stable or metastable.
[47] E. Helfand, J. Chem. Phys. **62**, 999 (1975).
[48] Q. Pike, F. A. Detcheverry, M. Müller, and J. J. de Pablo, J. Chem. Phys. **131**, 084903 (2009).
[49] F. A. Detcheverry, G. Liu, P. F. Nealey, and J. J. de Pablo, Macromolecules **43**, 3446 (2010).
[50] This value is slightly larger than that obtained directly from $\langle R_0^2/M \rangle$ for the experimental systems according to Ref. [51], $R_g \approx 5.8$ nm. Similar discrepancies were observed in other block copolymer systems, e.g., Ref. [52].
[51] L. J. Fetters, D. J. Lohse, D. Richter, T. A. Witten, and A. Zirkel, Macromolecules **27**, 4639 (1994).
[52] K. Mori, H. Tanaka, H. Hasegawa, and T. Hashimoto, Polymer **30**, 1389 (1989).
[53] A. Knoll, L. Tsarkova, and G. Krausch, Nano Lett. **7**, 843 (2007).
[54] S. Park and L. A. Tsarkova, Macromolecules **50**, 6840 (2017).